Interference Mitigation for Indoor Optical Attocell Networks using Angle Diversity Receiver

Interference Mitigation for Indoor Optical Attocell Networks Using an Angle Diversity Receiver

Zhe Chen, *Member, IEEE*, Dushyantha A. Basnayaka, *Senior Member, IEEE*, Xiping Wu, *Member, IEEE*, and Harald Haas, *Fellow, IEEE*

***Abstract*—In this paper, interference mitigation techniques based on angle diversity receivers (ADRs) are studied for optical attocell networks. Consisting of multiple photodiodes (PDs), an ADR requires appropriate signal combining schemes in order to mitigate intercell interference (ICI) in optical attocell networks. Four signal combining schemes, namely select best combining, equal gain combining, maximum ratio combining, and optimum combining are investigated. To further mitigate ICI, a novel double-source cell configuration with two transmission modes is also proposed. Results show that the systems with ADRs significantly outperform those with single-PD receivers in terms of signal-to-interference-plus-noise ratio (SINR). Also, compared to the conventional single-source cell configuration, the double-source cell configuration can provide an SINR improvement of over 20 dB. Furthermore, an analytical framework is proposed to analyze the performance of optical attocell networks with ADRs, where different propagation scenarios such as line-of-sight and nonline-of-sight are considered. The accuracy of the proposed analytical model is validated by Monte Carlo simulations.**

***Index Terms*—Angle diversity receiver, double-source cell configuration, optical attocell network, signal combining scheme, theoretical analysis, visible light communication.**

I. Introduction

IN RECENT years, the number of mobile devices in use has increased tremendously. As predicted in the latest Cisco Visual Networking Index (VNI), global mobile data traffic is expected to reach 24.3 exabytes per month by 2019 [1]. In order to alleviate the congested data traffic in existing radio frequency (RF) systems, visible light communication (VLC) technology has emerged as a promising alternative [2]. Recently, researchers have shown that VLC can achieve high data rates [3]. In particular, a single-colour light-emitting diode (LED) can achieve transmission speeds in excess of 10 Gbps [4]. Compared with RF communications, VLC can provide a much wider spectrum, which is licence-free. Also, it is intrinsically safe to use VLC in electromagnetic interference (EMI) sensitive environments [5], such as aircrafts, hospitals and oil refineries.

Cellular networks can achieve a higher area spectral efficiency (ASE) by efficient frequency reuse [6]. In a cellular network, the minimum distance between two access points (APs) is strictly limited to mitigate ICI. In the RF domain, a femtocell has a minimum cell diameter of 10 m [7]. An RF AP normally emits signals with wide beams, and thus ICI inevitably increases as the cell size decreases. In contrast, the light beams from LEDs are intrinsically narrow in VLC, and optical APs can be densely deployed without causing strong ICI [8]. Therefore, an optical cell size in the order of 1 m is achievable. In comparison with RF femtocell networks, optical cellular networks can achieve a better bandwidth reuse and a higher ASE [9]. In an indoor scenario, each lighting device can act as a VLC AP. A network consisting of multiple VLC APs is referred to as an optical attocell network.

Although optical attocell networks can offer several advantages over conventional RF cellular networks, their performance is still limited by ICI especially at cell-edge areas. The commonly used ICI mitigation techniques include fractional frequency reuse (FFR) [10] and joint transmission (JT) [11]. They have been proven to be able to improve signal quality for cell-edge users. In [12], a space division multiple access (SDMA) scheme using angle diversity transmitters was proposed. This method can mitigate ICI by generating concentrated light beams to users at different positions.

In this study, a novel ICI mitigation technique is proposed on the basis of an ADR, which consists of multiple narrow field-of-view (FOV) PDs with different orientations. In previous studies [13]–[17], the VLC systems with optical ADRs are analysed at the link level. This paper is focused on the system-level performance of optical attocell networks with ADRs. Four signal combining schemes namely select best combining (SBC), equal gain combining (EGC), maximum ratio combining (MRC) and optimum combining (OPC) are studied. Moreover, a novel double-source cell configuration with two transmission modes is proposed to improve SINR performance. The criteria for selecting the transmission mode in different deployment scenarios is also proposed. Finally, an analytical framework is developed to evaluate the performance of ADRs in hexagonal optical attocell networks. To the best of the authors' knowledge, this is the first

Manuscript received July 21, 2017; revised April 1, 2018; accepted April 8, 2018. Date of publication June 18, 2018; date of current version July 19, 2018. The work of H. Haas and D. A. Basnayaka was supported by the Engineering and Physical Sciences Research Council (EPSRC) under Established Career Fellowship Extension EP/R007101/1 (Go-by-Light). The work of H. Haas and X. Wu was supported by the EPSRC under Grant EP/L020009/1 (TOUCAN). *(Corresponding author: Harald Haas.)*

Z. Chen was with the Institute for Digital Communications, Li-Fi R&D Centre, School of Engineering, The University of Edinburgh, Edinburgh EH8 9YL, U.K., He is now with Fujitsu R&D Centre Co., Ltd., Beijing 100027, China (e-mail: chenzhe@cn.fujitsu.com).

D. A. Basnayaka, X. Wu, and H. Haas are with the Institute for Digital Communications, Li-Fi R&D Centre, School of Engineering, The University of Edinburgh, Edinburgh EH8 9YL, U.K. (e-mail: d.basnayaka@ed.ac.uk; xiping.wu@ed.ac.uk; h.haas@ed.ac.uk).

Color versions of one or more of the figures in this paper are available online at http://ieeexplore.ieee.org.

Digital Object Identifier 10.1109/JLT.2018.2848221

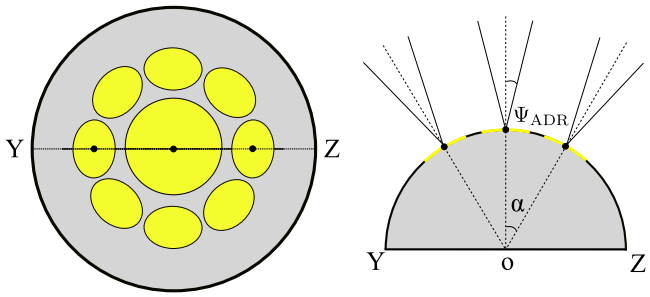

Fig. 1. The shape of an ADR (9 PDs).

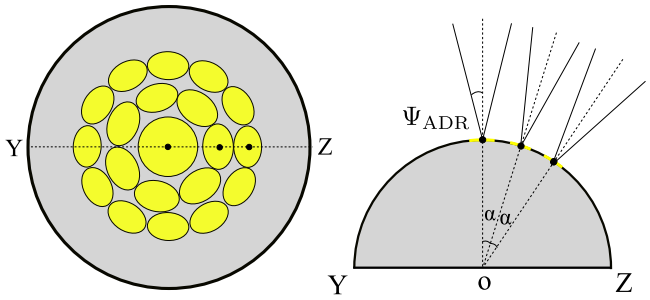

Fig. 2. The shape of an ADR (20 PDs).

time that ADRs have been used to achieve low ICI in optical attocell networks. Preliminary results of this study have been presented in [18] and [19]. This paper includes a detailed system model, an analytical framework of attocell networks with ADRs, double-source cell configuration and extended simulation results.

The remainder of this paper is organised as follows. Section II introduces the system model. Different signal combining schemes for ADRs are discussed in Section III. The concept of the optical double-source cell is proposed in Section IV. Theoretical analysis of optical attocell networks is presented in Section V. The results and discussions are presented in Section VI. Finally, conclusions are drawn in Section VII.

II. System Model

A. Optical Receivers

In this study, three different types of optical receivers are considered in optical attocell networks. The first type is a single-PD receiver, which only has one upward-pointing PD with a FOV of Ψ_{single}. The second type is an ADR with 9 PDs. As shown in Fig. 1, this ADR has 1 upward-pointing PD surrounded by a ring of 8 PDs. The third type is an ADR with 20 PDs as shown in Fig. 2. In this type, there are 1 upward-pointing PD and two rings of PDs. The numbers of PDs in the inner and outer rings are 7 and 12, respectively. On an ADR, the FOV of each PD is identical and is denoted by Ψ_{ADR}. In addition, as shown in Figs. 1 and 2, α is defined as the tilted angle between the neighbouring rings. This parameter is designed in a way that minimises the overlap between the coverage areas of the PDs.

For a fair comparison, the overall coverage area of each optical receiver is set to be the same.

In optical attocell networks, ICI can be reduced by adding PDs on an optical receiver, especially when these PDs have different directions. This is because: i) with a fixed overall coverage area, the FOV of each PD becomes narrower as the number of PDs increases. A PD of a narrow FOV can effectively reject the line-of-sight (LOS) ICI from neighbouring APs; ii) since the nature of light reflections is dispersive, a PD element with narrow FOV can significantly mitigate non-line-of-sight (NLOS) ICI because most of the reflected light can be rejected; iii) as the number of PDs on an optical receiver increases, the granularity of the receiver increases. This results in a better capability of suppressing ICI.

B. Optical Propagation Model

The index of an AP is denoted by $a = 1, 2, ..., N_{\mathrm{AP}}$ and N_{AP} is the total number of APs. Also, the index of PDs is denoted by $p = 1, 2, ..., N_{\mathrm{PD}}$ and N_{PD} is the total number of PDs on an ADR. The electrical signal received by PD p is expressed in (1) [20], where the optical-to-electric conversion efficiency is denoted by τ; a_{d} is the index of the desired AP; $h_{a_{\mathrm{d}},p}(t)$ is the channel impulse response between AP a_{d} and PD p; $h_{a,p}(t)$ is the channel impulse response between AP a and PD p; $s_a(t)$ is the instantaneous power transmitted by AP a; the noise power at the receiver is denoted by $n_{\mathrm{rx}}(t)$; $\otimes$ is a convolution operator.

$$y_p(t) = \tau s_{a_{\mathrm{d}}}(t) \otimes h_{a_{\mathrm{d}},p}(t) + \sum_{a=1, a\neq a_{\mathrm{d}}}^{N_{\mathrm{AP}}} \tau s_a(t) \otimes h_{a,p}(t) + n_{\mathrm{rx}}(t). \tag{1}$$

Assuming that the effective symbol duration of the system is much longer than the duration of the channel impulse response, (1) can be rewritten as:

$$y_p(t) = \tau s_{a_{\mathrm{d}}}(t) H_{a_{\mathrm{d}},p} + \sum_{a=1, a\neq a_{\mathrm{d}}}^{N_{\mathrm{AP}}} \tau s_a(t) H_{a,p} + n_{\mathrm{rx}}(t), \tag{2}$$

where $H = \int_{\infty}^{-\infty} h(t)\mathrm{d}t$ is the channel direct current (DC) gain. A detailed discussion about the validity of (2) is given in Appendix VII-A.

C. Channel Gain

In this study, both LOS and NLOS paths are considered. The overall channel DC gain is given by:

$$H = H_{\mathrm{LOS}} + \sum_{l=1}^{N_{\mathrm{ref}}} H_{\mathrm{NLOS}}^{l}, \tag{3}$$

where l is the order of reflections; N_{ref} is the total number of light reflections that are taken into account.

1) LOS Propagation: The channel DC gain of the LOS path is [20]:

$$H_{\mathrm{LOS}} = \frac{(m+1)A_{\mathrm{eff}}}{2\pi d^2} \cos^m(\phi) \cos(\psi) \mathrm{rect}\left(\frac{\psi}{2\Psi_{\mathrm{fov}}}\right), \tag{4}$$

where d represents the distance from a transmitter to a receiver; the angle of irradiance is denoted by ϕ; the FOV of the optical receiver is $\Psi_{\rm fov}$; the Lambertian order of the transmitter is $m = -1/\log_2(\cos(\Phi_{\rm tx}))$ and $\Phi_{\rm tx}$ is the half-intensity radiation angle; the angle of light incidence at the receiver is denoted by ψ; the rectangular function is denoted by $\mathrm{rect}(\cdot)$; the effective signal collection area $A_{\rm eff}$ is given by:

$$A_{\rm eff} = A_{\rm p} G \frac{n_{\rm ref}^2}{\sin^2(\Psi_{\rm fov})}, \tag{5}$$

where the refractive index of the receiver optics is denoted by $n_{\rm ref}$; G represents the signal transmission gain of the optical filter; the physical area of the PD is $A_{\rm p}$.

2) NLOS Propagation: The NLOS channel gain can be calculated by dividing the reflective surface into small areas [21]. Each area reflects a fraction of incident light energy. Typically, the fraction of the reflected light energy is related to the reflection coefficient of the surface material. This complex behaviour of light is mathematically modelled as follows.

A typical NLOS propagation consists of three parts. The first one is the light path from an optical transmitter to the qth reflective area. The channel gain of this path is:

$$L_{1,q} = \frac{(m+1)\Delta A}{2\pi d_{q,\rm tx}^2} \cos^m(\phi)\cos(\psi), \tag{6}$$

where the area of the reflecting surface element is ΔA. $d_{q,\rm tx}$ is the distance between the optical transmitter and the qth reflective area.

In the second part, the qth reflective area is regarded as a light source and the pth reflective area is regarded as a receiver. The corresponding channel gain can be written as:

$$L_{l,p} = \sum_{q=1}^{Q} \frac{\rho_q (n+1)\cos^n(\phi)\cos(\theta)\Delta A}{2\pi d_{p,q}^2} L_{l-1,q}, \tag{7}$$

where l denotes the total number of light reflections. The distance between the reflective areas p and q is $d_{p,q}$. The total number of reflective areas is Q. The reflection coefficient of the reflective area q is denoted by ρ_q; the Lambertian order of the reflective area is n. In this study, the half-intensity radiation angle of the reflective area $\theta_{\rm ref}$ is set to be $60^{\rm o}$.

In the last part, the light propagates from the last reflective area to a receiver. The channel gain of this part is given in (8), where $d_{\rm rx,p}$ denotes the distance between the qth reflective area and the optical receiver.

$$H_{\rm NLOS}^{l} = \sum_{p=1}^{Q} L_{l,p} \frac{\rho_p (n+1)\Delta A}{2\pi d_{\rm rx,p}^2} \cos^n(\phi)\cos(\psi)\mathrm{rect}\left(\frac{\psi}{\Psi_{\rm fov}}\right). \tag{8}$$

III. Signal Combining Schemes for ADR

Four signal combining schemes, SBC, EGC, MRC and OPC, are described in this section. Each user chooses the desired AP that provides the strongest signal:

$$a_{\rm d} = \underset{a}{\mathrm{argmax}} \sum_{p=1}^{N_{\rm PD}} \left|H_{a,p}\right|^2. \tag{9}$$

The ADR combines the signals received by the PDs. According to (1), the received electrical signal sample is given by:

$$z(t) = \sum_{p=1}^{N_{\rm PD}} w_p y_p(t). \tag{10}$$

SINR is an important metric to evaluate the link quality and capacity. According to [20], the SINR of the desired user after signal combining is given by:

$$\gamma = \frac{\left(\sum_{p=1}^{N_{\rm PD}} \tau P_{\rm tx} w_p H_{a_{\rm d},p}\right)^2}{\sum_{p=1}^{N_{\rm PD}} w_p^2 N_0 B + \sum_{a=1,a\neq a_{\rm d}}^{N_{\rm AP}} \left(\tau P_{\rm tx} \sum_{p=1}^{N_{\rm PD}} w_p H_{a,p}\right)^2}, \tag{11}$$

where w_p is the weight of PD p, which is different in different combining schemes; the communication bandwidth is B; the additive white Gaussian noise (AWGN) power spectral density is N_0; $P_{\rm tx}$ is the optical transmission power of a VLC AP which is defined as the standard deviation of $s(t)$:

$$P_{\rm tx} = \lim_{T\to\infty} \sqrt{\frac{1}{T}\int_0^T (s(t)-\bar{s})^2 \mathrm{d}t}, \tag{12}$$

where T denotes the time duration over which the standard deviation of $s(t)$ is calculated, and $\bar{s}$ is given by:

$$\bar{s} = \frac{1}{T}\int_0^T s(t)\mathrm{d}t. \tag{13}$$

If $N_{\rm PD}$ is set to 1, (11) reduces to the electrical SINR of a single-PD receiver.

A. SBC Scheme

In SBC, the PD with the highest received signal-to-noise ratio (SNR) is selected to receive light signals. The index of the desired PD is determined by:

$$p_{\rm d} = \underset{p}{\mathrm{argmax}} \frac{\left(\tau P_{\rm tx} H_{a_{\rm d},p}\right)^2}{N_0 B}. \tag{14}$$

The weight of each PD is given by:

$$w_p = \begin{cases} 1 & p = p_{\rm d} \\ 0 & \text{otherwise.} \end{cases} \tag{15}$$

According to (14), only the knowledge of channel state information (CSI) from the desired cell to a user is required. The knowledge of CSI from the other interfering APs to the user is not needed. A switch is required to select the signals from the desired PD.

B. EGC Scheme

The EGC simply combines the signals received by all PDs with equal weights, i.e., $w_p = 1$ for all PDs. An adder is required in the signal combining circuit. No knowledge of CSI is required. Due to the sum of the optical power from multiple PDs, EGC can receive a higher optical power than SBC. However, EGC fails to mitigate ICI since the weight of each PD is identical. This might result in poor system performance.

C. MRC Scheme

In MRC, the weight w_p is proportional to the SNR received by each PD:

$$w_p = \frac{\left(\tau P_{\mathrm{tx}} H_{a_{\mathrm{d}},p}\right)^2}{N_0 B}. \tag{16}$$

Similar to SBC, MRC only requires the CSI from the desired AP to the user of interest. The weight of each PD can be adjusted according to the knowledge of CSI. Hence, by using MRC, the desired signals can be enhanced and the interference and noise can be mitigated.

D. OPC Scheme

If there is no ICI, MRC can provide the optimum SNR [23]. However, in the proposed system, interference from the neighbouring APs can be received in both LOS and NLOS propagations. There is a strong correlation between the interfering signals received by different PDs. This degrades the overall performance of MRC. In order to further improve system performance, OPC is used, which was firstly proposed for RF communications in [23]. In this study, OPC is applied to optical attocell networks. By using OPC, ICI can be mitigated by using an interference-plus-noise correlation matrix. The weight of each PD in OPC is given by:

$$\mathbf{w} = \xi \mathbf{R}_{nn}^{-1} \mathbf{u}_{a_{\mathrm{d}}}, \tag{17}$$

where the signals received from the desired AP a_{d} is $\mathbf{u}_{a_{\mathrm{d}}} = [\tau P_{\mathrm{tx}} H_{a_{\mathrm{d}},1}, \tau P_{\mathrm{tx}} H_{a_{\mathrm{d}},2}, \ldots, \tau P_{\mathrm{tx}} H_{a_{\mathrm{d}},N_{\mathrm{PD}}}]^T$; $\mathbf{w} = [w_1, w_2, \ldots, w_{N_{\mathrm{PD}}}]^T$ is a vector containing the weights; ξ is a scaling factor; the interference-plus-noise correlation matrix $\mathbf{R}_{nn}$ can be represented by:

$$\mathbf{R}_{nn} = N_0 B \mathbf{I} + \sum_{a \neq a_{\mathrm{d}}} \left[\mathbf{u}_a \mathbf{u}_a^T\right]. \tag{18}$$

In (18), $\mathbf{u}_a = [\tau P_{\mathrm{tx}} H_{a,1}, \tau P_{\mathrm{tx}} H_{a,2}, \ldots, \tau P_{\mathrm{tx}} H_{a,N_{\mathrm{PD}}}]^T$ is the vector of the signals received from AP a, with $\mathbf{I}$ being the identity matrix.

Compared with SBC and MRC, OPC requires the CSI knowledge from not only the desired cell but also all other interfering cells. By cancelling the correlated interference at each PD, OPC is expected to have better SINR performance than MRC.

IV. Double-Source Optical Cell

In previous studies, each cell in optical attocell networks is equipped with a single AP at the cell centre. This intrinsic way of cell deployment is not always optimal when ADRs are employed. In order to further exploit the advantage of ADRs, a novel double-source cell configuration is proposed.

As shown in Fig. 3, there are two APs, termed the positive AP and the negative AP, in each optical cell. The time domain signal transmitted by these APs are denoted by $s_{\mathrm{pos}}(t)$ and $s_{\mathrm{neg}}(t)$, respectively, with a dynamic range from 0 to s_{H}. Two data transmission modes, mode A and mode B, are developed for the double-source cell configuration.

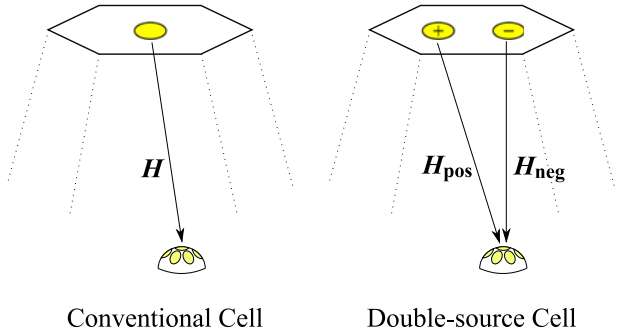

Fig. 3. The layouts of different cell configurations.

A. Mode A

In mode A, within the same optical cell, the information carried by $s_{\mathrm{pos}}(t)$ is the same as the information carried by $s_{\mathrm{neg}}(t)$. The relationship between $s_{\mathrm{pos}}(t)$ and $s_{\mathrm{neg}}(t)$ is given by:

$$s_{\mathrm{neg}}(t) = s_{\mathrm{H}} - s_{\mathrm{pos}}(t). \tag{19}$$

According to (12), the negative AP and the positive AP have the same transmission power, which is computed by:

$$\mathrm{P_{tx}} = \sqrt{\mathrm{E}\left[(s_{\mathrm{pos}}(t) - \mathrm{E}[s_{\mathrm{pos}}(t)])^2\right]}. \tag{20}$$

In order to conduct a fair comparison, the double-source cell configuration the same total transmission power as the single-source cell configuration. In other words, the transmission power of each node in the double-source cell configuration is half of that in the single-source cell configuration.

Also, the transmission power is assumed to be the same for all APs. For a single optical cell, the received optical signal at a PD is represented as:

$$s_{\mathrm{sum}}(t) = s_{\mathrm{pos}}(t) H_{\mathrm{pos}} + s_{\mathrm{neg}}(t) H_{\mathrm{neg}}, \tag{21}$$

where H_{neg} is the channel gain between the negative AP and a PD; H_{pos} is the channel gain between the positive AP and a PD. The received optical power at a PD is obtained by:

$$\mathrm{P_{rx}} = \sqrt{\mathrm{E}\left[(s_{\mathrm{sum}}(t) - \mathrm{E}[s_{\mathrm{sum}}(t)])^2\right]}. \tag{22}$$

Substituting (21) into (22), it gives:

$$\mathrm{P_{rx}} = \sqrt{\mathrm{E}\left[(s_{\mathrm{pos}}(t) - \mathrm{E}[s_{\mathrm{pos}}(t)])^2\right]}\,|H_{\mathrm{pos}} - H_{\mathrm{neg}}|. \tag{23}$$

Combining with (20), (23) can be rewritten as:

$$\mathrm{P_{rx}} = \mathrm{P_{tx}} \Delta H, \tag{24}$$

where ΔH denotes the difference between H_{pos} and H_{neg}.

It can be observed from (22) that the received signal power increases with ΔH. In general, the desired cell is close to a receiver and the interfering cells are much further away. As illustrated in Fig. 4, a receiver is underneath its desired cell and ΔH is large. This is because the PD can hardly receive LOS signals from the two APs at the same time due to the narrow FOV. Therefore between H_{pos} and H_{neg}, only one channel appears as the LOS channel gain in (21). Since ΔH is large, the received

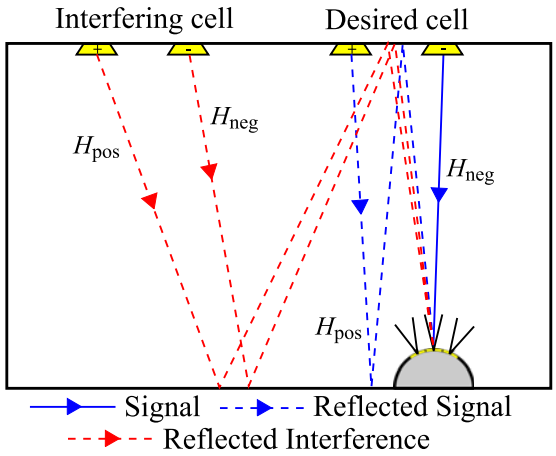

Fig. 4. The schematic diagram of a double-source cell configuration.

signals increase accordingly. It is also shown in Fig. 4 that when a receiver is far from an interfering cell, the channel gains H_{pos} and H_{neg} are both NLOS. The difference between them is small and the received interference is attenuated accordingly. Therefore the double-source cell configuration can increase the signal power from the desired cell and suppress the signal power from interfering cells. Moreover, the double-source cell configuration is practical and energy-efficient when implemented. A realistic differential LED driver for the double-source cell configuration has been made [24].

B. Mode B

Transmission mode A can effectively suppress interference. However, mode A requires an optical receiver that has the ability to separate the signals of the positive and negative APs in the desired cell. Otherwise the SINR performance would be significantly degraded, especially at the cell centre. In order to facilitate the receivers that cannot distinguish the signals of the positive and negative APs, another transmission mode, mode B, is proposed. In mode B, the relationship between $s_{\text{neg}}(t)$ and $s_{\text{pos}}(t)$ can be expressed as:

$$s_{\text{neg}}(t) = s_{\text{pos}}(t). \tag{25}$$

This means both APs transmit identical signals. In order to optimise the system performance of the double-source cell configuration, certain criteria for selecting the transmission mode is necessary. This will be discussed in Section VI.

V. Performance Analysis

In this section, an analytical framework of analysing the system performance of optical attocell networks is presented. For simplicity, a 7-cell model is considered. Also, each optical cell is assumed to be hexagonal.

A. Simplified NLOS Propagation Model

Firstly, a simplification of the NLOS model is required. As described in [25], high-order reflections are considered in the conventional models, resulting in high computational complexity. However, there is no need to consider high order reflections in an optical attocell network. This can be explained in Fig. 5. A receiver with a narrow FOV can reject direct interference ($O \rightarrow C$) from neighbouring cells. Furthermore, this receiver can also block first-order reflections ($O \rightarrow D \rightarrow C$). Second-order reflections are the dominant source for ICI because the other high-order reflections attenuate significantly and thus are negligible. Hence, only the second-order reflections ($O \rightarrow A \rightarrow B \rightarrow C$) are considered in the simplified model. The propagation path of second order reflections can be separated into two parts: part I ($O \rightarrow A \rightarrow B$) and part II ($B \rightarrow C$).

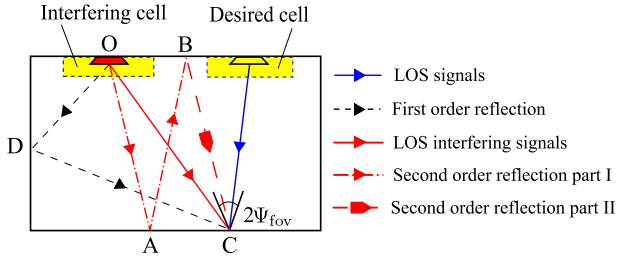

Fig. 5. The propagation model in optical attocell network.

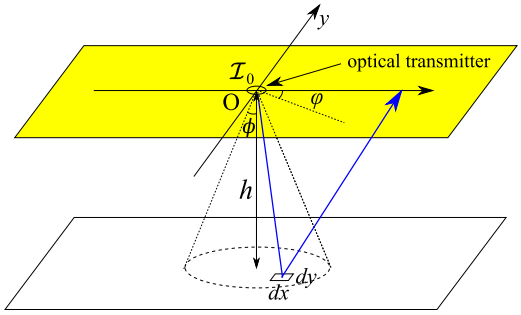

Fig. 6. The conventional propagation model of the part I of second-order reflections.

1) Part I: In this part, light signals are considered to be emitted from an LED at point O. These signals bounce off the floor and back to the ceiling (see Fig. 6). The optical power density of the reflected light at point O has the maximum value, which is calculated as follows:

$$\mathcal{I}_0 = \frac{C(m+1)(n+1)}{4\pi^2 h^{-(m+n+2)}} \iint_{\text{floor}} \frac{dxdy}{(x^2+y^2+h^2)^{(m+n+6)/2}}. \tag{26}$$

The coefficients x and y are given by:

$$\begin{cases} x = h\tan(\phi)\cos(\varphi) \\ y = h\tan(\phi)\sin(\varphi), \end{cases} \tag{27}$$

where ϕ is the angle of irradiance and φ is the azimuth angle. Then the intensity density at point O can be obtained by:

$$\mathcal{I}_0 = \frac{C(m+1)(n+1)}{2\pi h^2(m+n+4)}, \tag{28}$$

where the coefficient $C = \rho_{\text{floor}}\rho_{\text{ceiling}}P_{\text{tx}}$; and the reflection coefficient of the floor and ceiling are ρ_{floor} and ρ_{ceiling},

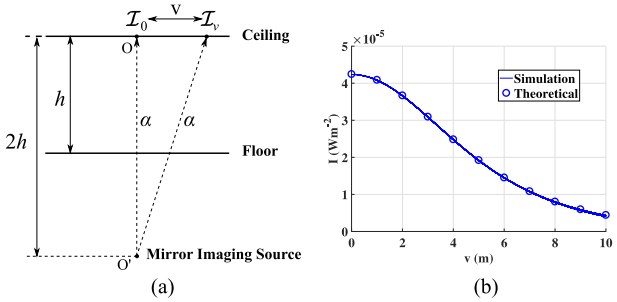

Fig. 7. The simplified propagation model of the part I of second-order reflections. (a) Simplified reflection model. (b) Reflected optical power density at horizontal different distances.

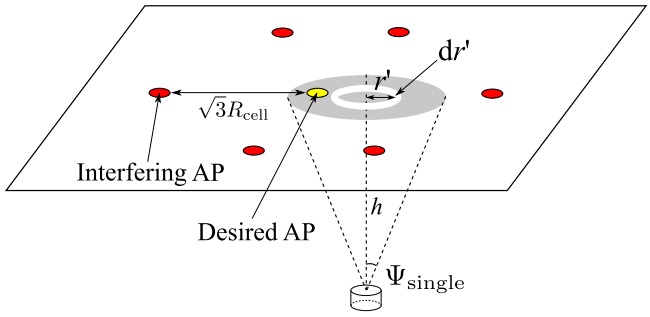

Fig. 8. The simplified propagation model of the part II of second-order reflections.

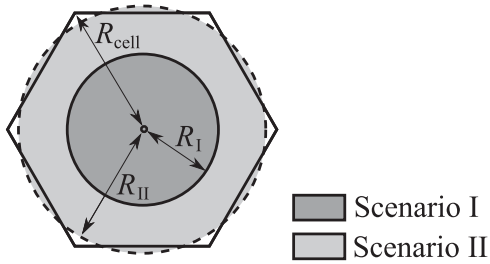

Fig. 9. The regions of scenario I and scenario II.

respectively; also, J is the Jacobian determinant of the coordinate conversion which can be represented as:

$$J = \det\left(\left[\frac{\partial x}{\partial \phi}, \frac{\partial x}{\partial \varphi}; \frac{\partial y}{\partial \phi}, \frac{\partial y}{\partial \varphi}\right]\right). \tag{29}$$

In the simplified model, $\mathcal{I}_0$ is used to estimate the optical power density at other points on the ceiling. The optical power density of a point on the ceiling is related to its horizontal distance to point O. The trend of attenuation is approximated by the model shown in Fig. 7(a). It is assumed that the optical power is emitted from a mirror imaging source O' and the distance between O and O' is $2h$. At point O, the optical power intensity is assumed to be the same as in the conventional model. The attenuation factor is denoted by α. The optical power density, denoted by $\mathcal{I}_v$, is then derived by:

$$\mathcal{I}_v = \mathcal{I}_0 \left(\frac{2h}{\sqrt{v^2 + 4h^2}}\right)^{\alpha}, \tag{30}$$

where v is the horizontal distance from an arbitrary point to point O. The attenuation factor α is chosen to minimise the difference between the proposed simplified model and the conventional model. In this study, the transmitter semi-angle is chosen to be 60^o and α is set to be 4.8. Fig. 7(b) shows that the simplified model matches the conventional one well. In the simplified model, $\mathcal{I}_v$ can be calculated in a closed form in (30). This means that the simplified model can significantly reduce the computational complexity in comparison with the conventional model.

2) Part II: In this part, the light reflected from the ceiling is transmitted to a receiver (see Fig. 8). Since the FOV of the receiver is narrow, only the light reflected from the grey area on the ceiling can be captured by the receiver. Also, the optical power intensity of the reflected light in the grey area can be considered constant. In a 7-cell optical attocell network, the NLOS interference to one AP is sourced from its six neighbouring APs. The distance between an interfering AP to the centre of the desired cell is $\sqrt{3}R_{\text{cell}}$, where R_{cell} denotes the cell's radius. The total NLOS interference is computed by:

$$\mathcal{I}_{\text{NLOS}}(\Psi_{\text{single}}) = 6\left[\int_0^{h\tan(\Psi_{\text{single}})} \tau \mathcal{I}_v 2\pi r' H(r') \mathrm{d}r'\right]^2. \tag{31}$$

With straightforward integral calculations, (31) can be rewritten as:

$$\mathcal{I}_{\text{NLOS}}(\Psi_{\text{single}}) = 6\left[\tau \mathcal{I}_v A_{\text{eff}} \sin^2(\Psi_{\text{single}})\right]^2 \Big|_{v=\sqrt{3}R_{\text{cell}}}. \tag{32}$$

B. SINR Statistic of Conventional Single-PD Receiver

The service quality in optical attocell networks is determined by the statistic of the received SINR. In this study, the cumulative distribution function (CDF) of received SINR is derived to evaluate the performance of optical attocell networks. The simplified NLOS propagation model is applied in the evaluation because the conventional model is intractable. Depending on the user's position, the statistical analysis of a single-PD receiver falls into two categories: scenario I and scenario II, as shown in Fig. 9. For simplicity, the boundary of scenario II is assumed to be a circle, which has the same area as the original cell, i.e. $R_{\text{II}} \approx 0.91 R_{\text{cell}}$.

1) Scenario I: As shown in Fig. 9, users are uniformly distributed at the cell centre. No LOS interference from the neighbouring cells can be captured (see Fig. 10). The horizontal distance between an active user and its desired cell centre is defined as r. The probability density function (PDF) of r is:

$$f_{\text{I}}(r) = \frac{2r}{R_{\text{I}}^2}, \quad (0 \le r \le R_{\text{I}}), \tag{33}$$

where R_{I} is the radius of the circular region of scenario I. By considering the geometric relationship between the parameters:

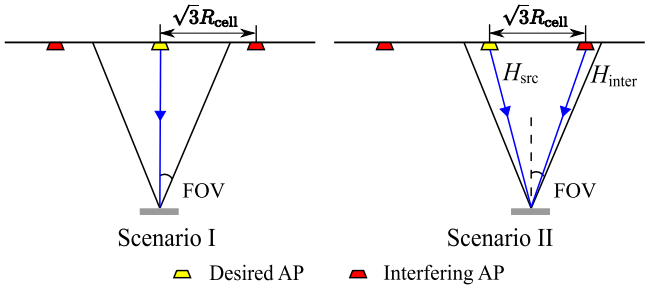

Fig. 10. The layout of scenario I and scenario II.

$d = h/\cos(\phi), \cos(\phi) = h/\sqrt{h^2+r^2}, \psi = \phi$, (4) is:

$$H(r, \Psi_{\text{single}}) = \frac{(m+1)A_{\text{eff}}(\Psi_{\text{single}})}{2\pi h^2}\left(\frac{h}{\sqrt{h^2+r^2}}\right)^{m+3}, \tag{34}$$

where Ψ_{single} is the FOV of a single-PD receiver. Assuming that an attocell network is an interference limited system, the SINR is:

$$\gamma(r) = \frac{\left(\tau P_{\text{tx}} H(r, \Psi_{\text{single}})\right)^2}{\mathcal{I}_{\text{NLOS}}(\Psi_{\text{single}}) + N_0 B} \approx \frac{\left(\tau P_{\text{tx}} H(r, \Psi_{\text{single}})\right)^2}{\mathcal{I}_{\text{NLOS}}(\Psi_{\text{single}})}. \tag{35}$$

The PDF of SINR for scenario I is:

$$f_{\text{I}}(\gamma) = \begin{cases} \dfrac{h^2}{(m+3)R_{\text{I}}^2}\gamma_0^{\frac{1}{m+3}}\gamma^{-\frac{m+4}{m+3}} & \gamma_{\text{I}} \le \gamma \le \gamma_0 \\ 0 & \text{otherwise}, \end{cases} \tag{36}$$

where γ_0 is the maximum SINR at the cell centre ($r = 0$), which is:

$$\gamma_0 = \frac{\left(\tau P_{\text{tx}} H(0, \Psi_{\text{single}})\right)^2}{\mathcal{I}_{\text{NLOS}}(\Psi_{\text{single}})}; \tag{37}$$

and γ_{I} is the minimum SINR at the boundary of the region of scenario I ($r = R_{\text{I}}$):

$$\gamma_{\text{I}} = \frac{\left(\tau P_{\text{tx}} H(R_{\text{I}}, \Psi_{\text{single}})\right)^2}{\mathcal{I}_{\text{NLOS}}(\Psi_{\text{single}})}. \tag{38}$$

The closed-form CDF of the SINR for the scenario I is:

$$F_{\text{I}}(\gamma) = \begin{cases} 0 & \gamma < \gamma_{\text{I}} \\ \dfrac{h^2}{R_{\text{I}}^2}\gamma_0^{\frac{1}{m+3}}\left(\gamma_{\text{I}}^{-\frac{1}{m+3}} - \gamma^{-\frac{1}{m+3}}\right) & \gamma_{\text{I}} \le \gamma \le \gamma_0 \\ 1 & \gamma > \gamma_0. \end{cases} \tag{39}$$

2) Scenario II: As shown in Fig. 9, users are uniformly distributed in the region of scenario II. LOS interference from the neighbouring cell can be received (see Fig. 10). The PDF of r in scenario II is:

$$f_{\text{II}}(r) = \frac{2r}{R_{\text{II}}^2 - R_{\text{I}}^2}, \quad (R_{\text{I}} \le r \le R_{\text{II}}), \tag{40}$$

where R_{II} is the outer radius of the region of scenario II.

In this scenario, since the magnitude of the LOS ICI is a few orders of magnitude higher than the NLOS ICI and noise [26], NLOS ICI and noise are assumed to be negligible. Hence, the SINR of the system can be approximated by:

$$\gamma(r) \approx \left(\frac{h^2+\tilde{r}^2}{h^2+(\sqrt{3}R_{\text{cell}} - r)^2}\right)^{-(m+3)}, \tag{41}$$

where $H_{\text{src}}(r)$ is the DC gain of the link from the desired AP to the optical receiver; $H_{\text{inter}}(r)$ is the link from the interfering AP to the optical receiver; $\tilde{r} = \sqrt{3}R_{\text{cell}} - (R_{\text{I}} + R_{\text{II}})/2$. The PDF of the SINR for the scenario II is:

$$f_{\text{II}}(\gamma) = \begin{cases} \dfrac{h^2+\tilde{r}^2}{(m+3)(R_{\text{II}}^2 - R_{\text{I}}^2)}\gamma^{-\frac{m+2}{m+3}} & 1 \le \gamma \le \gamma_{\text{I}}' \\ 0 & \text{otherwise}, \end{cases} \tag{42}$$

and the CDF of the SINR for the scenario II is:

$$F_{\text{II}}(\gamma) = \begin{cases} 0 & \gamma < 1 \\ \dfrac{h^2+\tilde{r}}{R_{\text{II}}^2 - R_{\text{I}}^2}\left(-1 + \gamma^{\frac{1}{m+3}}\right) & 1 \le \gamma \le \gamma_{\text{I}}' \\ 1 & \gamma > \gamma_{\text{I}}', \end{cases} \tag{43}$$

and γ_{I}' is also the SINR that exists at the boundary of region I ($r = R_{\text{I}}$). Unlike γ_{I} in (38), γ' represents the SINR of an optical receiver that captures the LOS interference from the AP in the vicinity. The difference between (38) and (44) is due to the cut-off effect of the receiver's FOV. The coefficient γ_{I}' is derived as follows:

$$\gamma_{\text{I}}' = \left(\frac{h^2+\tilde{r}^2}{h^2+(\sqrt{3}R_{\text{cell}} - R_{\text{I}})^2}\right)^{-(m+3)}. \tag{44}$$

3) Overall Theoretical Performance: Similar to the derivation for scenario I and scenario II, the SINR CDF of a single-PD receiver in optical attocell networks can be derived. The PDF of r is given as follows:

$$f_{\text{overall}}(r) = \frac{2r}{R_{\text{II}}^2}, \quad (0 \le r \le R_{\text{II}}). \tag{45}$$

Similar to (36) and (42), the PDF of the SINR γ, is derived as follows:

$$f_{\text{overall}}(\gamma) = \begin{cases} \dfrac{h^2+\tilde{r}^2}{(m+3)R_{\text{II}}^2}\gamma^{-\frac{m+2}{m+3}} & 1 \le \gamma \le \gamma_{\text{I}}' \\ \dfrac{h^2}{(m+3)R_{\text{II}}^2}\gamma_0^{\frac{1}{m+3}}\gamma^{-\frac{m+4}{m+3}} & \gamma_{\text{I}} \le \gamma \le \gamma_0 \\ 0 & \text{otherwise}, \end{cases} \tag{46}$$

where $\gamma_{\text{I}} > \gamma_{\text{I}}'$. It is notable that the PDF of SINR γ follows a bimodal distribution (see Fig. 11). The PDF of SINR consists of two regions, high SINR and low SINR. The high SINR region corresponds to scenario I (cell centre). In the cell centre, the limited FOV of a PD can reject the LOS interference

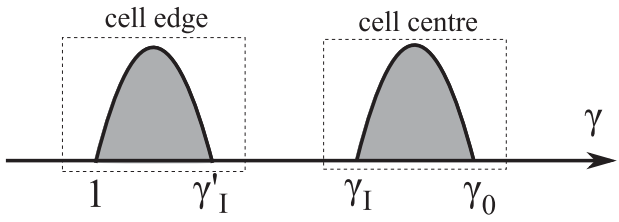

Fig. 11. The bimodal distribution of the SINR PDF of a single-PD receiver.

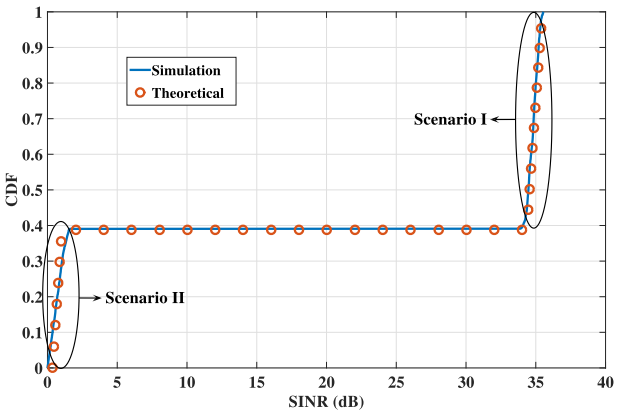

Fig. 12. The CDF of the received SINR when conventional single-PD receivers are used.

from neighbouring cells which means only NLOS interference is presented. This results in a high received SINR. The low SINR region corresponds to scenario II (cell edge). Strong LOS ICI at the cell edge results in low received SINR. It is notable that there is a sharp separation between the low and high SINR regions. This is because of the cut-off effect stemmed from the FOV-limited optical receiver. According to (36) and (42), the PDF can then be calculated as:

$$f_{\text{overall}}(\gamma) = \begin{cases} \dfrac{R_{\text{II}}^2 - R_{\text{I}}^2}{R_{\text{II}}^2} f_{\text{II}}(\gamma) & 1 \le \gamma \le \gamma' \\ \dfrac{R_{\text{I}}^2}{R_{\text{II}}^2} f_{\text{I}}(\gamma) & \gamma_{\text{I}} \le \gamma \le \gamma_0 \\ 0 & \text{otherwise.} \end{cases} \tag{47}$$

The CDF of the SINR can be obtained by:

$$F_{\text{overall}}(\gamma) = \int_{-\infty}^{\gamma} f_{\text{overall}}(\gamma)\, \mathrm{d}\gamma. \tag{48}$$

Combining with (47), (48) can be rewritten as:

$$F_{\text{overall}}(\gamma) = \frac{R_{\text{I}}^2}{R_{\text{II}}^2} F_{\text{I}}(\gamma) + \frac{R_{\text{II}}^2 - R_{\text{I}}^2}{R_{\text{II}}^2} F_{\text{II}}(\gamma). \tag{49}$$

The SINR performance of a single-PD receiver via numerical simulation and theoretical analysis are shown in Fig. 12. The theoretical results show a close match to the simulation results which verifies the accuracy of the theoretical model.

C. SINR Statistics of Angle Diversity Receiver

The theoretical tools developed for analysing single-PD receivers can be generalised to ADRs. For simplicity, it is assumed that each PD on an ADR points to a different direction and there is no overlap between the aperture of each PD. This means that one PD can establish at most one LOS link with a desired AP.

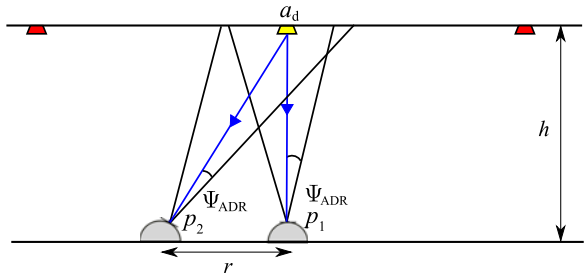

Fig. 13. A generalisation of scenario I. The desired AP is in yellow and the interfering APs are in red.

1) SBC: As shown in Fig. 13, the user in the cell centre selects the upward pointing PD p_1 to achieve the best SINR performance. Similar to (35), the SINR of that user can be derived as follows:

$$\gamma_{\text{SBC,centre}}(r) = \frac{\left(\tau P_{\text{tx}} H(r, \Psi_{\text{ADR}})\right)^2}{\mathcal{I}_{\text{NLOS}}(\Psi_{\text{ADR}})}, \tag{50}$$

where Ψ_{ADR} is the FOV of PDs on an ADR; $\mathcal{I}_{\text{NLOS}}(\Psi_{\text{ADR}})$ is the NLOS interference received by p_1.

The user at the cell edge selects PD p_2 to achieve the best SINR, which is obtained by:

$$\gamma_{\text{SBC,edge}}(r) = \frac{\left(\tau P_{\text{tx}} H(r, \Psi_{\text{ADR}})\right)^2}{\mathcal{I}'_{\text{NLOS}}(\Psi_{\text{ADR}})}, \tag{51}$$

where $\mathcal{I}'_{\text{NLOS}}$ is the NLOS interference received by p_2. According to [27], when p_1 and p_2 have identical FOV, $\mathcal{I}_{\text{NLOS}}(\Psi_{\text{ADR}}) = \mathcal{I}'_{\text{NLOS}}(\Psi_{\text{ADR}})$. This means that the SINR of the optical receiver can be represented by (50) in both cell centre and cell edge area. Therefore, the PDF of the SINR γ, can be approximated as follows:

$$f_{\text{SBC}}(\gamma) = \begin{cases} \dfrac{h^2 (\gamma_{0,\text{SBC}})^{\frac{1}{m+3}}}{(m+3) R_{\text{II}}^2} \gamma^{-\frac{m+4}{m+3}} & \gamma_{\text{II,SBC}} \le \gamma \le \gamma_{0,\text{SBC}} \\ 0 & \text{otherwise,} \end{cases} \tag{52}$$

where $\gamma_{0,\text{SBC}}$ is the SINR at $r = 0$:

$$\gamma_{0,\text{SBC}} = \frac{\left(\tau P_{\text{tx}} H(0, \Psi_{\text{ADR}})\right)^2}{\mathcal{I}_{\text{NLOS}}(\Psi_{\text{ADR}})}, \tag{53}$$

and $\gamma_{\text{II,SBC}}$ is the SINR at $r = R_{\text{II}}$:

$$\gamma_{\text{II,SBC}} = \frac{\left(\tau P_{\text{tx}} H(R_{\text{II}}, \Psi_{\text{ADR}})\right)^2}{\mathcal{I}_{\text{NLOS}}(\Psi_{\text{ADR}})}. \tag{54}$$

The CDF of the SINR for the SBC is given in (55) as shown at the bottom of this page.

Furthermore, it can be shown that the received SINR increases when a user moves vertically closer to the AP (such as in a

$$F_{\text{SBC}}(\gamma_{\text{dB}}) = \begin{cases} 0 & \text{if } \gamma < \gamma_{\text{II,SBC}} \\ \dfrac{h^2}{R_{\text{II}}^2} \gamma_{0,\text{SBC}}^{\frac{1}{m+3}} \left(\gamma_{\text{II,SBC}}^{-\frac{1}{m+3}} - \gamma^{-\frac{1}{m+3}}\right) & \text{if } \gamma_{\text{II,SBC}} \le \gamma \le \gamma_{0,\text{SBC}} \\ 1 & \text{if } \gamma > \gamma_{0,\text{SBC}} \end{cases} \tag{55}$$

walking scenario). In (50) and (51), the received SINR of a user consists of two parts: received signal power and NLOS interference. According to [27], NLOS interference remains the same even if the position of a user changes vertically. This means that the SINR is only a function of received signal power. According to (4), the received signal power is proportional to $1/d^2$. Also, the distance between an AP to a PD, d, increases when the user moves vertically downwards. Hence, the received SINR of a user increases when the user moves vertically upwards.

2) EGC: In cell centres, the received signal of a user using EGC is similar to that of SBC. This is because, as discussed in the assumption, only one of the PDs can receive the LOS signal from the desired cell. However, since the weights of all PDs are identical, the received NLOS ICI increases when the number of PDs on the receiver increases. Therefore, the SINR can be approximated as follows:

$$\gamma_{\mathrm{EGC,centre}}(r) = \frac{\left(\tau P_{\mathrm{tx}} H(r, \Psi_{\mathrm{ADR}})\right)^2}{M^2 \mathcal{I}_{\mathrm{NLOS}}(\Psi_{\mathrm{ADR}})}, \tag{56}$$

where M denotes the number of neighbouring cells.

The SINR of cell edge users is similar to (41):

$$\gamma_{\mathrm{EGC,edge}}(r) = \frac{\left(\tau P_{\mathrm{tx}} H_{\mathrm{src}}(r, \Psi_{\mathrm{ADR}})\right)^2}{\left(\tau P_{\mathrm{tx}} H_{\mathrm{inter}}(r, \Psi_{\mathrm{ADR}})\right)^2}. \tag{57}$$

Similar to the derivation in Section V-B, the CDF of SINR, γ in EGC can be approximated as follows:

$$F_{\mathrm{EGC}}(\gamma) = \frac{R_{\mathrm{I}}^2}{R_{\mathrm{II}}^2} F_{\mathrm{EGC,centre}}(\gamma) + \frac{R_{\mathrm{II}}^2 - R_{\mathrm{I}}^2}{R_{\mathrm{II}}^2} F_{\mathrm{EGC,edge}}(\gamma), \tag{58}$$

where $F_{\mathrm{EGC,edge}}(\gamma) = F_{\mathrm{II}}(\gamma)$ and $F_{\mathrm{EGC,centre}}(\gamma)$ is given in (59) as shown at the bottom of this page. Here, $\gamma_{0,\mathrm{EGC}}$ is the SINR at the cell centre ($r = 0$):

$$\gamma_{0,\mathrm{EGC}} = \frac{\left(\tau P_{\mathrm{tx}} H(0, \Psi_{\mathrm{single}})\right)^2}{M^2 \mathcal{I}_{\mathrm{NLOS}}(\Psi_{\mathrm{ADR}})}; \tag{60}$$

and $\gamma_{\mathrm{I,EGC}}$ is the SINR at the boundary of scenario I ($r = R_{\mathrm{I}}$):

$$\gamma_{\mathrm{I,EGC}} = \frac{\left(\tau P_{\mathrm{tx}} H(R_{\mathrm{I}}, \Psi_{\mathrm{single}})\right)^2}{M^2 \mathcal{I}_{\mathrm{NLOS}}(\Psi_{\mathrm{ADR}})}. \tag{61}$$

3) MRC: In MRC, different weights will be allocated to different PD elements according to their SNR. Therefore, the SINR of a user when using MRC can be represented by:

$$\gamma_{\mathrm{MRC}} = \frac{\left(\tau P_{\mathrm{tx}} \sum_{p=1}^{N_{\mathrm{PD}}} w_p H_{a_{\mathrm{d}},p}\right)^2}{\mathcal{I}_{\mathrm{NLOS,MRC}}}, \tag{62}$$

where $\mathcal{I}_{\mathrm{NLOS,MRC}}$ is the NLOS interference component when MRC is used. According to the assumption that only one PD can establish a LOS link to the source AP, it can be concluded that:

$$w_{p_{\mathrm{d}}} \gg w_{p \neq p_{\mathrm{d}}}. \tag{63}$$

The LOS links have the highest SINR, and thus contributes the most to the received signal. Therefore, (62) can be approximated as follows:

$$\gamma_{\mathrm{MRC}}(r) \approx \frac{\left(\tau P_{\mathrm{tx}} H(r, \Psi_{\mathrm{ADR}})\right)^2}{\mathcal{I}_{\mathrm{NLOS}}(\Psi_{\mathrm{ADR}})}. \tag{64}$$

After the approximation, (64) and (50) are identical. Hence, the approximated CDF of the SINR for MRC is: $F_{\mathrm{MRC}}(\gamma) = F_{\mathrm{SBC}}(\gamma)$.

4) OPC: OPC mitigates the NLOS ICI by exploiting CSI of NLOS interference. The SINR of OPC is:

$$\gamma_{\mathrm{OPC}} = \frac{\left(\sum_{p=1}^{N_{\mathrm{PD}}} \tau w_p P_{\mathrm{tx}} H_{a_{\mathrm{d}},p}\right)^2}{\mathcal{I}_{\mathrm{NLOS,OPC}} + \sum_{p=1}^{N_{\mathrm{PD}}} w_p^2 N_0 B}, \tag{65}$$

where $\mathcal{I}_{\mathrm{NLOS,OPC}}$ is the NLOS interference component of OPC. Similar to MRC, the SINR of OPC can be further approximated as follows:

$$\gamma_{\mathrm{OPC}}(r) = \frac{\left(\tau P_{\mathrm{tx}} w_{p_{\mathrm{d}}} H(r, \Psi_{\mathrm{ADR}})\right)^2}{\mathcal{I}_{\mathrm{NLOS,OPC}} + \sum_{p=1}^{N_{\mathrm{PD}}} w_p^2 N_0 B}. \tag{66}$$

The proof of (66) is provided in Appendix VII-B, and the upper bound of the OPC is derived as follows:

$$\gamma_{\mathrm{OPC,UB}}(r) = \frac{\left(\tau P_{\mathrm{tx}} H(r, \Psi_{\mathrm{ADR}})\right)^2}{N_0 B} > \gamma_{\mathrm{OPC}}(r). \tag{67}$$

The proof of (67) is provided in Appendix VII-B. The CDF of the SINR for the OPC upper bound is denoted by $F_{\mathrm{OPC,UB}}(\gamma)$, which is given in (68) as shown at the bottom of this page. where $\gamma_{\mathrm{II,OPC}}$ can be represented as follows:

$$\gamma_{\mathrm{II,OPC}} = \frac{\left(\tau P_{\mathrm{tx}} H(R_{\mathrm{II}}, \Psi_{\mathrm{ADR}})\right)^2}{N_0 B}, \tag{69}$$

$$F_{\mathrm{EGC,centre}}(\gamma) = \begin{cases} 0 & \text{if} \quad \gamma < \gamma_{\mathrm{I,EGC}} \\ \dfrac{h^2}{R_{\mathrm{I}}^2} \gamma_{0,\mathrm{EGC}}^{\frac{1}{m+3}} \left(\gamma_{\mathrm{I,EGC}}^{-\frac{1}{m+3}} - \gamma^{-\frac{1}{m+3}}\right) & \text{if} \quad \gamma_{\mathrm{I,EGC}} \leq \gamma \leq \gamma_{0,\mathrm{EGC}} \\ 1 & \text{if} \quad \gamma > \gamma_{0,\mathrm{EGC}} \end{cases} \tag{59}$$

$$F_{\mathrm{OPC,UB}}(\gamma) = \begin{cases} 0 & \text{if} \quad \gamma < \gamma_{\mathrm{II,OPC}} \\ \dfrac{h^2}{R_{\mathrm{II}}^2} \gamma_{0,\mathrm{OPC}}^{\frac{1}{m+3}} \left(\gamma_{\mathrm{II,OPC}}^{-\frac{1}{m+3}} - \gamma^{-\frac{1}{m+3}}\right) & \text{if} \quad \gamma_{\mathrm{II,OPC}} \leq \gamma \leq \gamma_{0,\mathrm{OPC}} \\ 1 & \text{if} \quad \gamma > \gamma_{0,\mathrm{OPC}} \end{cases} \tag{68}$$

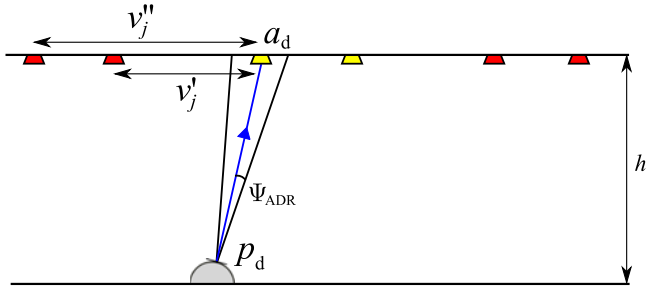

Fig. 14. The usage of SBC in double source cell configuration.

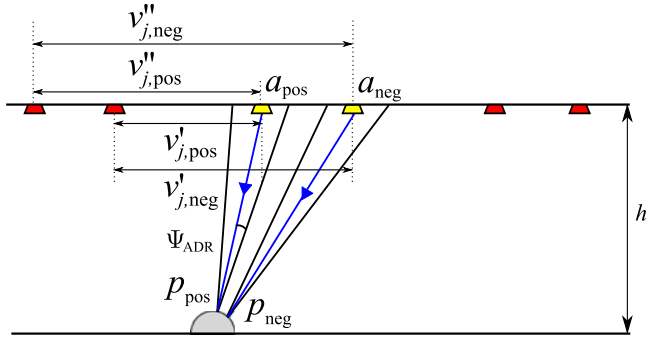

Fig. 15. The usage of MRC in double source cell configuration.

and $\gamma_{0,\mathrm{OPC}}$ can be represented as follows:

$$\gamma_{0,\mathrm{OPC}} = \frac{\left(\tau P_{\mathrm{tx}} H(0, \Psi_{\mathrm{ADR}})\right)^2}{N_0 B}. \tag{70}$$

D. SINR Statistics of Double-Source Cell Configuration

In double-source cell configuration, the distance between two APs in the same cell is designed in such a way that no PD on an ADR can simultaneously receive LOS light signals from the two APs in the desired cell. In this section, SINR performance of ADR in double-source cell configuration using mode A is analysed. Since positive and negative APs are close to the cell centre, their LOS channel gains are calculated by (34).

1) SBC: As illustrated in Fig. 14, the ADR using SBC chooses one AP to establish a LOS link. Similar to (50), the SINR of a user can be approximated as follows:

$$\gamma_{\mathrm{SBC}}^{\mathrm{double}}(r) = \frac{\left(\frac{1}{2} P_{\mathrm{tx}} \tau H(r, \Psi_{\mathrm{ADR}})\right)^2}{\mathcal{I}_{\mathrm{NLOS,SBC}}^{\mathrm{double}}(\Psi_{\mathrm{ADR}})}. \tag{71}$$

Note that the transmission power of each node in the double-source cell configuration is half of that in the single-source cell configuration. According to (22) and (31), the total NLOS interference, $\mathcal{I}_{\mathrm{NLOS,SBC}}^{\mathrm{double}}(\Psi_{\mathrm{ADR}})$, using SBC in double-source cell configuration is derived as follows:

$$\mathcal{I}_{\mathrm{NLOS,SBC}}^{\mathrm{double}}(\Psi_{\mathrm{ADR}}) = A_{\mathrm{eff}}^2 \tau^2 \sin^2(\Psi_{\mathrm{ADR}}) \sum_j \left| I_{v_j'} - I_{v_j''} \right|^2, \tag{72}$$

where j is the index of interfering optical cells; v_j' represents the distance from the desired AP to a positive AP in interfering cell j; v_j'' represents the distance from the desired AP to a negative AP in interfering cell j. The CDF of the SINR for SBC in double-source cell configuration can be derived using a method similar to the analysis of the single-source cell configuration in Section V-B.

2) MRC: As illustrated in Fig. 15, ADR using MRC can establish two LOS links with both positive and negative APs. The SINR of an active user can therefore yield:

$$\gamma_{\mathrm{MRC}}^{\mathrm{double}} = \frac{\left(\frac{1}{2}\tau P_{\mathrm{tx}} \left(w_{p_{\mathrm{pos}}} H_{a_{\mathrm{pos}},p_{\mathrm{pos}}} + w_{p_{\mathrm{neg}}} H_{a_{\mathrm{neg}},p_{\mathrm{neg}}}\right)\right)^2}{\mathcal{I}_{\mathrm{NLOS,MRC}}^{\mathrm{double}}(\Psi_{\mathrm{ADR}})}, \tag{73}$$

where $\mathcal{I}_{\mathrm{NLOS,MRC}}^{\mathrm{double}}(\Psi_{\mathrm{ADR}})$ is the power of NLOS ICI in double-source cell configuration when MRC is used. Since the desired positive AP and the desired negative AP in the same cell are close to each other and the transmission power of them is the same, the relationship between the channel gain $H_{a_{\mathrm{pos}},p_{\mathrm{pos}}}$ and $H_{a_{\mathrm{neg}},p_{\mathrm{neg}}}$ is:

$$H_{a_{\mathrm{pos}},p_{\mathrm{pos}}} \approx H_{a_{\mathrm{neg}},p_{\mathrm{neg}}}. \tag{74}$$

According to (16) and (74), it can be derived that the relationship between the weight of PDs is:

$$w_{p_{\mathrm{pos}}} \approx w_{p_{\mathrm{neg}}}. \tag{75}$$

To this end, (73) can be approximated as follows:

$$\gamma_{\mathrm{MRC,double}}(r) \approx \frac{\left(\tau P_{\mathrm{tx}} H(r, \Psi_{\mathrm{ADR}})\right)^2}{\mathcal{I}'^{\mathrm{double}}_{\mathrm{NLOS,MRC}}(\Psi_{\mathrm{ADR}})}, \tag{76}$$

where, according to (22) and (31), $\mathcal{I}'^{\mathrm{double}}_{\mathrm{NLOS,MRC}}(\Psi_{\mathrm{ADR}})$ can be calculated as follows:

$$\mathcal{I}'^{\mathrm{double}}_{\mathrm{NLOS,MRC}}(\Psi_{\mathrm{ADR}}) = A_{\mathrm{eff}}^2 \tau^2 \sin^2(\Psi_{\mathrm{ADR}}) \times \sum_j \left(\left| \mathcal{I}_{v'_{j,\mathrm{pos}}} - \mathcal{I}_{v''_{j,\mathrm{pos}}} \right| + \left| \mathcal{I}_{v'_{j,\mathrm{neg}}} - \mathcal{I}_{v''_{j,\mathrm{neg}}} \right| \right)^2, \tag{77}$$

where $v'_{j,\mathrm{pos}}$ is the horizontal distance between a positive AP in interfering cell j and the positive AP in the desired cell; $v'_{j,\mathrm{neg}}$ is the horizontal distance between a positive AP in the interfering cell j and the negative AP in the desired cell; $v''_{j,\mathrm{pos}}$ is the horizontal distance between a negative AP in interfering cell j and the positive AP in the desired cell; $v''_{j,\mathrm{neg}}$ is the horizontal distance between a negative AP in the interfering cell j and the negative AP in the desired cell.

3) OPC: Similar to MRC, the LOS signals of OPC are captured by two PDs that can establish LOS links with desired APs. Therefore, the SINR of OPC in double-source cell configuration is:

$$\gamma_{\mathrm{OPC}}^{\mathrm{double}} = \frac{\left(\frac{1}{2}\tau P_{\mathrm{tx}} \left(w_{p_{\mathrm{pos}}} H_{a_{\mathrm{pos}},p_{\mathrm{pos}}} + w_{p_{\mathrm{neg}}} H_{a_{\mathrm{neg}},p_{\mathrm{neg}}}\right)\right)^2}{\mathcal{I}_{\mathrm{NLOS,OPC}}^{\mathrm{double}} + \sum_{p=1}^{N_{\mathrm{PD}}} w_p^2 N_0 B}, \tag{78}$$

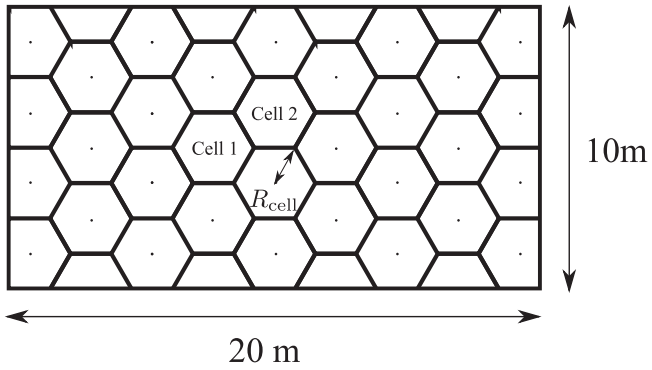

Fig. 16. The layout of a $20 \times 10 \times 4$ m room implementing an optical attocel network. Two optical APs are denoted as Cell 1 and Cell 2.

where $\mathcal{I}_{\text{NLOS,OPC}}^{\text{double}}$ is the NLOS interference component of OPC. The SINR of OPC in the double-source cell configuration can be approximated as:

$$\gamma_{\text{OPC}}^{\text{double}}(r) \approx \frac{\left(\frac{1}{2}\tau P_{\text{tx}}\left(w_{p_{\text{pos}}} + w_{p_{\text{neg}}}\right) H(r, \Psi_{\text{ADR}})\right)^2}{\mathcal{I}_{\text{NLOS,OPC}}^{\text{double}} + \sum_{p=1}^{N_{\text{PD}}} w_p^2 N_0 B}. \tag{79}$$

According to (79), the upper bound of the OPC in the double-source cell configuration is:

$$\gamma_{\text{OPC,UB}}^{\text{double}}(r) = \frac{\left(\tau P_{\text{tx}} H(r, \Psi_{\text{ADR}})\right)^2}{2N_0 B} > \gamma_{\text{OPC}}^{\text{double}}(r). \tag{80}$$

The proof for (80) is provided in Appendix VII-C. By comparing (67) and (80), it is notable that the noise level doubles when the double-source configuration is used. The double source system employs two PDs to receive the LOS signal in an ADR receiver configuration. As a result, the noise power caused by the amplifier circuit is doubled. This means that the SINR performance is expected to be degraded by 3 dB compared to OPC.

VI. Results and Discussions

In this section, analytical and simulation results are compared and discussed. As shown in Fig. 16, simulations are conducted in a $20 \times 10 \times 4\,\text{m}$ room, and the total number of light reflections is $N_{\text{ref}} = 4$. The system with single-PD receivers is considered to be a baseline. For fairness, the FOV is assumed to be the same for all receivers. The FOV of the single-PD receiver is set to be 22^{o}. For the ADR with 9 PDs, α and Ψ_{ADR} are set as 8.5^{o} and 15.5^{o}, respectively. For the ADR with 20 PDs, α and Ψ_{ADR} are set to be 6^{o} and 10.5^{o}, respectively. In the double source cell configuration, the distance between the two APs in the desired cell requires careful set up so that the ADR can distinguish the light signals from these APs. When a 9-PD receiver is used, the distance between positive and negative APs is set to be 0.7 m. When a 20-PD receiver is used, this distance changes to 0.5 m. The reflection coefficients of the walls, the ceiling, and the floor are 0.8, 0.8 and 0.2, respectively [28]. The total transmission power of each optical cell is assumed to be 1 W.

TABLE I
Simulation Parameters

Radius of an optical cell, R_{cell}	1.5 m
Responsivity, τ	1 A/W
The gain of the optical filter, G	1
Refractive index, n	1.5
Transmitter half-intensity radiation angle, θ_{tx}	60°
The physical area of a PD, A_{p}	5 mm^2
Modulation Bandwidth, B	20 MHz
AWGN spectral density, N_0	1×10^{-21} A/Hz

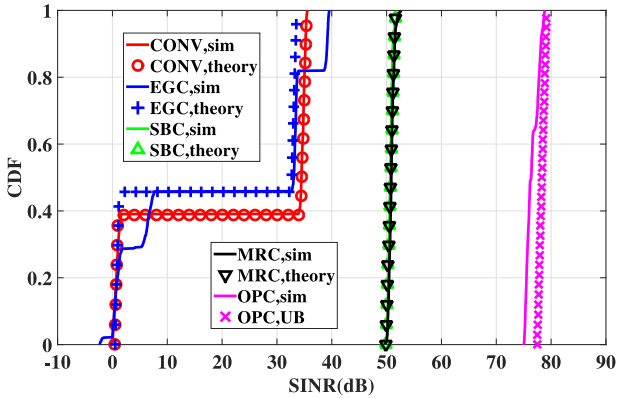

Fig. 17. The CDF of the achieved SINR at a 9-PD ADR in the conventional single-source cell configuration.

Other simulation parameters are listed in Table I. With respect to the theoretical analysis, a seven-cell configuration is considered with the same parameters as above.

A. Convention Single-Source Cell Configuration

Fig. 17 shows the SINR performance for the single-source cell configuration when an ADR with 9 PDs is used. Similar to a single-PD receiver, the SINR CDF of a 9-PD ADR with EGC also has bimodal characteristics. The reason for this is that the EGC-ADR combines the received light signals with the same weight and cannot suppress the LOS ICI at the cell edge like a single PD receiver. The theoretical result in (58) accurately captures the SINR performance trends of the EGC receiver with some exceptions, like the 6 dB gaps in certain parts of the curves. This is because, in the numerical simulation, a LOS signal might be captured by two different PDs simultaneously, which doubles the received optical power.

The SINR performance of a 9-PD ADR with SBC is significantly better than a single-PD receiver. This is because the SBC chooses the PD that provides the highest channel gain. Due to the narrow FOV, this PD is free from LOS interference. This means the SBC can successfully avoid LOS ICI at the cell edges. From (31), it is notable that the NLOS interference decreases as the FOV of a PD decreases. Since the FOV of the selected PD is narrower than the single-PD receiver, the NLOS interference is significantly mitigated compared to the single-PD receiver. Also, numerical results closely match the theoretical results in (55), which proves the accuracy of the model.

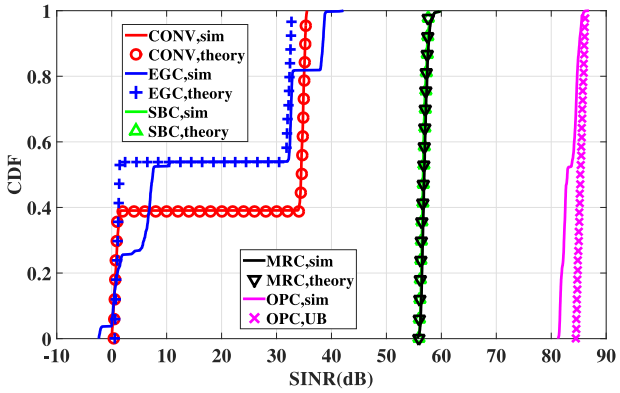

Fig. 18. The CDF of the achieved SINR at a 20-PD ADR in the conventional single-source cell configuration.

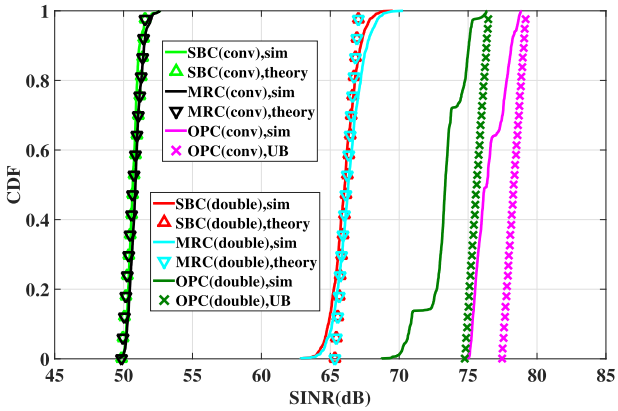

Fig. 19. The CDF of the achieved SINR at a 9-PD ADR.

The performance of the MRC is, as expected, nearly identical to the SBC. Due to the diffusive NLOS propagation paths, the interference signals received by each PD are correlated and the MRC is unable to suppress this interference. Therefore, the performance of the MRC is not optimal.

As shown in Fig. 17, the OPC has the best SINR performance among all signal combining schemes. By exploiting the interference-plus-noise correlation matrix, the OPC can generate the best weights for the ADR. These weights can effectively suppress the correlated NLOS interfering signals. Results show that OPC achieves over 20 dB improvement over SBC and MRC. The theoretical upper bound for the SINR performance of OPC in (68) is also closely comparable to the simulated SINR performance.

Fig. 18 shows the SINR performance for a single-source cell configuration with an ADR of 20 PDs. The SINR performance trend of EGC is similar to the performance of the previous scenario in Fig. 17. This is because the overall coverage area of the ADR remains unchanged when the number of receiver elements increases. In SBC and MRC, the SINR performance of a 20-PD ADR system exhibits a 5 dB improvement over a 9-PD ADR system. This is because each PD on the 20-PD ADR has a narrower FOV. A narrower FOV means less NLOS interference is captured. Therefore, the overall SINR performance improves. In OPC, interference from other cells is significantly suppressed. The main factor that affects the system performance is the magnitude of the received desired power. Since the receiver elements of a 20-PD ADR have a narrower FOV and higher concentration gain than the PDs in a 9-PD ADR, the 20-PD ADR can receive stronger light signals. Therefore, usually a 20-PD ADR performs better than a 9-PD ADR when OPC is used. Moreover, since the interference has been significantly suppressed by OPC, better SINR performance can be achieved by adopting an ADR with an advanced concentrator [29].

In summary, in single-source cell configuration, OPC exhibits the best post combining SINR performance in comparison with other signal combining schemes. However, OPC requires the knowledge of CSI not only from the desired cell but also from all other interfering cells. Compared with the OPC, SBC and MRC also achieve better SINR performance by simply using the knowledge of CSI from the desired cell.

B. Double-Source Cell Configuration

In this section, the performance of the SBC, MRC, and OPC are evaluated in the mode A double-source cell configuration. Fig. 19 shows the SINR performance for both the single-source and double-source cell configurations with 9 PDs ADRs. In SBC, the SINR performance improves significantly when double-source cell configuration is implemented. This is because the NLOS interference has been significantly mitigated when two sources in the interfering cells combine destructively at the ADR. Also, there is a close match between the numerical and analytical SINR results. For MRC, the SINR performance is nearly identical to the SINR performance of SBC. This result is also comparable to the theoretical result. It can also be observed that the post combining SINR performance of OPC in a double-source cell is 3 dB weaker than the SINR performance in a single-source cell. This is also consistent with the theoretical analysis. Usually, two signals coming from a double-source cell are captured by two PDs. Since two PDs are required for OPC to capture light signals in a double-source cell, the total noise power is doubled compared with a single-source cell.

Fig. 20 shows the SINR performance for both the single-source and double-source cell configurations with 20 PDs. The SINR performance trends in a way similar to the scenario of a 9-PDs ADR. For each signal combining scheme, at least 5 dB SINR improvement can be obtained by a 20-PD receiver compared with a 9-PD receiver. This is also consistent with the results in a single-source cell.

In double-source cell configuration, an important observation is that the SINR performance of SBC and MRC is close to the SINR performance of OPC, which can approach the performance of a ICI-free system. Compared with OPC, SBC and MRC require less knowledge of CSI. Hence, it is suitable for the implementation in practice.

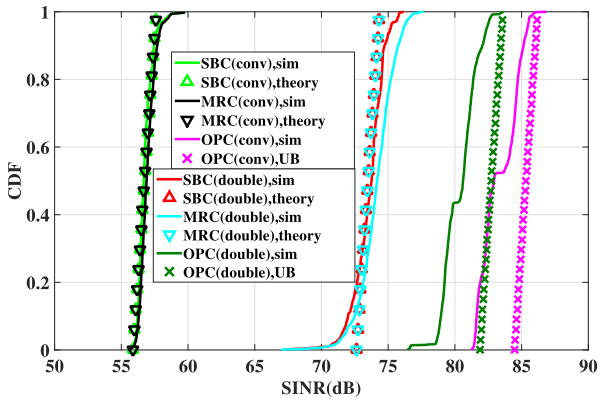

Fig. 20. The CDF of the achieved SINR at a 20-PD ADR.

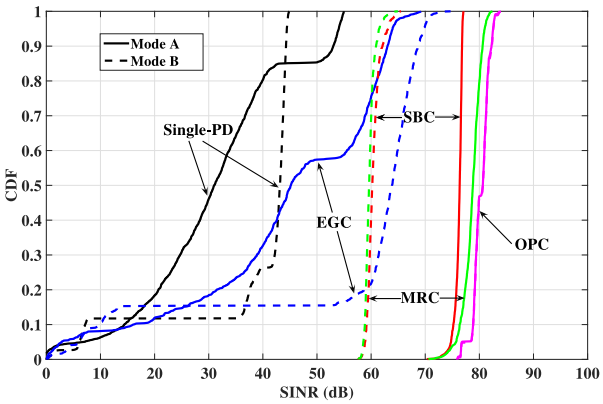

Fig. 21. The CDF of the achieved SINR at a 20-PD ADR in cell 1 when only one neighbouring cell is active.

C. Transmission Mode Selection in Double-Source Cell

Although double-source cell configuration using mode A shows a significant improvement, it may not be optimal in all scenarios. In practical optical attocell cell networks, several factors may affect the performance of mode A: a) due to the limitation of hardware, only a suboptimal signal combining scheme, such as EGC, can be applied to an optical receiver; b) active users equipped with a single-PD receiver will experience significant signal attenuation in the cell centre; c) when user density is low, only a few APs are active. This means the ICI is significantly reduced and the system can be regarded as noise-limited. In order to address these issues, transmission mode B is used as a complementary transmission mode for double-source attocell networks. To determine the criteria for the transmission modes, two cases are studied. One case is the interference-limited scenario. As illustrated in Fig. 16, only the desired cell (cell 1) and one interfering cell (cell 2) are activated in the room. Only the performance in the desired cell is evaluated. The other case is the noise-limited case. In this case, only one cell (cell 1) in the room is activated and evaluated.

Fig. 21 shows the SINR performance in cell 1 when one neighbouring interfering cell is active. In the single-PD receiver case, mode B achieves better performance. This is because a single-PD receiver cannot separate the signals from the positive AP and the negative AP. This results in a significant attenuation

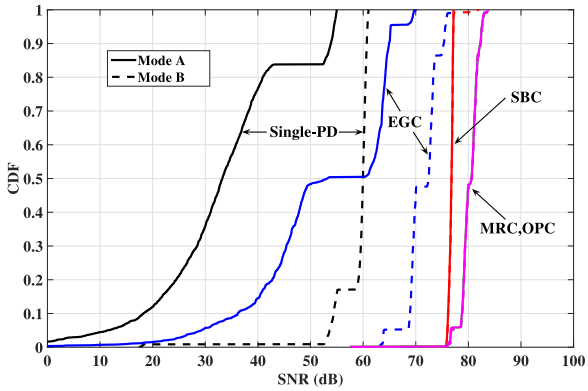

Fig. 22. The CDF of the achieved SNR at a 20-PD ADR in cell 1 when no neighbouring cell is active.

TABLE II
THE CRITERIA OF TRANSMISSION MODES SELECTION

	Single-PD	EGC	SBC	MRC	OPC
Interference	B	B	A	A	A or B
No Interference	B	B	A or B	A or B	A or B

of the received signal power, especially in the cell centre. The performance of EGC is similar to the single-PD receiver. As the EGC combines the signals from both positive and negative APs, the system performance degrades. In SBC and MRC, the SINR performance of mode A outperforms mode B since mode A can effectively mitigate ICI. In OPC, there is no difference between mode A and B. This is because OPC can effectively collect light energy and suppress correlated ICI by adjusting the weights for each PD.

Fig. 22 shows the CDF of SNR in cell 1 without ICI. For a single-PD receiver with EGC, there is a significant improvement when mode B is used. This is because mode B can boost the received signal power of a user. For SBC, since only one of the PDs can establish a data link, mode A has the same performance as mode B. For MRC, SNR performance of transmission mode A and transmission mode B is identical since the energy from both APs can be captured in both modes. Lastly, the SINR performance of OPC is identical to the SINR performance of MRC since there is no ICI. The criteria for selecting transmission modes in the double-source cell configuration is listed in Table II.

VII. CONCLUSIONS

This paper investigates interference mitigation techniques for indoor optical attocell networks with ADRs. Four different signal combining schemes, namely SBC, EGC, MRC and OPC are proposed and evaluated. The performance of ADR is also comprehensively compared with conventional single-PD receivers. A novel double-source cell configuration is proposed for the first time for ADR which can further mitigate ICI. Results show that an ADR outperforms a single-PD receiver in terms of SINR performance. In particular, an ADR using OPC achieves performance close to that of interference-free systems. However, OPC requires the knowledge of CSI from all optical APs in the

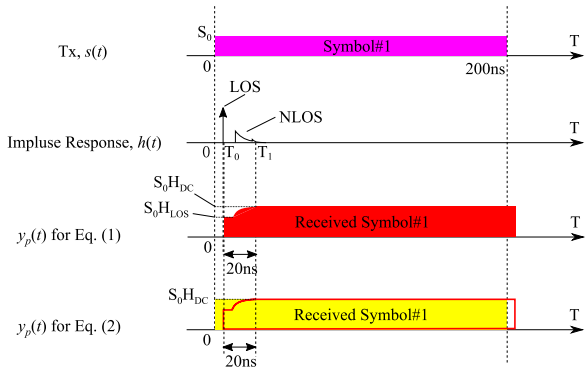

Fig. 23. Data transmission procedure.

network. In comparison, MRC and SBC can also provide better performance than a single-PD receiver and only the knowledge of CSI from the desired cell is required. Results also show that SBC and MRC can achieve better SINR performance in a mode A double-source cell configuration than in a single-source cell configuration. Mode B can provide better performance when a single-PD receiver or EGC-ADR are used in the double-source cell configuration. The criteria for selecting transmission modes in double-source attocell networks are determined. This work has shown that segmented optics in combination with intelligent signal combining techniques provides a powerful instrument to combat interference in optical attocell networks.

APPENDIX

A. Discussion of the Validity of (2)

In a realistic communication system, transmission power $s(t)$ remains constant within a symbol. As illustrated in Fig. 23, the value of Symbol#1 is S_0 and the symbol duration of Symbol#1 is 200 ns. A typical impulse response $h(t)$ is comprised of different components (see Fig. 23). The Dirac impulse represents a LOS component, with NLOS components being spread in time domain since they transmit through different paths from an AP to a PD. The LOS component occurs at T_0, and the duration of the impulse response is infinite in theory. However, the value of the impulse response decays significantly after a certain time, which is denoted by T_1. It can be observed that the peak value of the impulse response at T_0 is 10^4 higher than that at T_1. The time difference between T_0 and T_1 is defined as the effective time duration of the impulse response. According to [30], this effective time duration is around 20 ns.

The received signal $y(t)$ is a result of the convolution between $s(t)$ and $h(t)$. The value of $y(t)$ at T_0 is $S_0 H_{\mathrm{LOS}}$ and it saturates at T_1, which is $S_0 H_{\mathrm{DC}}$. Since the time duration of the symbol is much longer than the effective time duration of the impulse response, the value of the received symbol can be considered as constant, which is $S_0 H_{\mathrm{DC}}$. In (2), T_0 is ignored and the value of the received symbol is assumed as constant (see Fig. 23).

Since the symbol duration is 200 ns, the symbol rate is 5 Msymbol/s. Assuming 16-QAM modulation, the data rate of the system can be up to 20 Mbps. This means that (2) in this particular case would be applicable for single carrier systems which exhibit a data rate of up to 20 Mbps. Multicarrier systems such as orthogonal frequency division multiplexing (OFDM) are composed of multiple narrow band parallel transmission streams. Therefore, the same principles apply for higher data rates which scale with the available bandwidth [30].

B. The Proof of (66) and (67)

$$\gamma_{\mathrm{OPC}} = \frac{\tau^2 P_{\mathrm{tx}}^2 \left(w_{p_{\mathrm{d}}} H_{a_{\mathrm{d}},p_{\mathrm{d}}} + \sum_{p \neq p_{\mathrm{d}}} w_p H_{a_{\mathrm{d}},p} \right)^2}{\mathcal{I}_{\mathrm{NLOS,OPC}} + \sum_{p=1}^{N_{\mathrm{PD}}} w_p^2 N_0 B}. \tag{81}$$

The magnitude of the LOS channel is a few orders larger than the NLOS channel. Since only the desired PD a_{d} can establish LOS link with the desired AP:

$$H_{a_{\mathrm{d}},p_{\mathrm{d}}} \gg H_{a_{\mathrm{d}},p}. \quad (p \neq p_{\mathrm{d}}). \tag{82}$$

As mentioned, the OPC system is dominantly limited by interference. Neglecting the affect of noise, the SINR of OPC can be approximated as follows:

$$\begin{aligned}\gamma_{\mathrm{OPC}}(r) &\approx \frac{\left(\tau P_{\mathrm{tx}} w_{p_{\mathrm{d}}} H(r, \Psi_{\mathrm{ADR}})\right)^2}{\mathcal{I}_{\mathrm{NLOS,OPC}} + \sum_{p=1}^{N_{\mathrm{PD}}} w_p^2 N_0 B} \\ &= \frac{\left(\tau P_{\mathrm{tx}} w_{p_{\mathrm{d}}} H(r, \Psi_{\mathrm{ADR}})\right)^2}{\mathcal{I}_{\mathrm{NLOS,OPC}} + \sum_{p \neq p_{\mathrm{d}}} w_p^2 N_0 B + w_{p_{\mathrm{d}}}^2 N_0 B} \\ &< \frac{\left(\tau P_{\mathrm{tx}} w_{p_{\mathrm{d}}} H(r, \Psi_{\mathrm{ADR}})\right)^2}{w_{p_{\mathrm{d}}}^2 N_0 B}.\end{aligned} \tag{83}$$

While:

$$\begin{aligned}\gamma_{\mathrm{OPC,UB}}(r) &= \frac{\left(\tau P_{\mathrm{tx}} H(r, \Psi_{\mathrm{ADR}})\right)^2}{N_0 B} \\ &< \frac{\left(\tau P_{\mathrm{tx}} w_{p_{\mathrm{d}}} H(r, \Psi_{\mathrm{ADR}})\right)^2}{w_{p_{\mathrm{d}}}^2 N_0 B}.\end{aligned} \tag{84}$$

Therefore:

$$\gamma_{\mathrm{OPC}}(r) < \gamma_{\mathrm{OPC,UB}}(r). \tag{85}$$

C. The Proof of (80)

$$\begin{aligned}\gamma_{\mathrm{OPC}}^{\mathrm{double}}(r) &= \frac{\left(\frac{1}{2}\tau P_{\mathrm{tx}} \left(w_{p_{\mathrm{pos}}} + w_{p_{\mathrm{neg}}}\right) H(r, \Psi_{\mathrm{ADR}})\right)^2}{\mathcal{I}_{\mathrm{NLOS,OPC}}^{\mathrm{double}} + \sum_{p=1}^{N_{\mathrm{PD}}} w_p^2 N_0 B} \\ &< \frac{\left(\frac{1}{2}\tau P_{\mathrm{tx}} \left(w_{p_{\mathrm{pos}}} + w_{p_{\mathrm{neg}}}\right) H(r, \Psi_{\mathrm{ADR}})\right)^2}{\left(w_{p_{\mathrm{pos}}}^2 + w_{p_{\mathrm{neg}}}^2\right) N_0 B}\end{aligned} \tag{86}$$

Since:

$$(w_{p_{\mathrm{pos}}} - w_{p_{\mathrm{neg}}})^2 \geq 0. \tag{87}$$

We have:

$$w_{p_{\rm pos}}^2 + w_{p_{\rm neg}}^2 \geq 2 w_{p_{\rm pos}} w_{p_{\rm neg}}. \tag{88}$$

As both $w_{p_{\rm pos}}$ and $w_{p_{\rm neg}}$ are positive, it gives:

$$\frac{2 w_{p_{\rm pos}} w_{p_{\rm neg}}}{w_{p_{\rm pos}}^2 + w_{p_{\rm neg}}^2} \leq 1. \tag{89}$$

Therefore:

$$\begin{aligned} \frac{(w_{p_{\rm pos}} + w_{p_{\rm neg}})^2}{w_{p_{\rm pos}}^2 + w_{p_{\rm neg}}^2} &= 1 + \frac{2 w_{p_{\rm pos}} w_{p_{\rm neg}}}{w_{p_{\rm pos}}^2 + w_{p_{\rm neg}}^2}. \\ &\leq 2. \end{aligned} \tag{90}$$

Note that (86) can be rewritten as:

$$\gamma_{\rm OPC}^{\rm double}(r) < \frac{\left(w_{p_{\rm pos}} + w_{p_{\rm neg}}\right)^2}{w_{p_{\rm pos}}^2 + w_{p_{\rm neg}}^2} \times \frac{\left(\tau P_{\rm tx} H(r, \Psi_{\rm ADR})\right)^2}{4 N_0 B}. \tag{91}$$

Combining (90) and (91), we have:

$$\gamma_{\rm OPC}^{\rm double}(r) < \frac{\left(\tau P_{\rm tx} H(r, \Psi_{\rm ADR})\right)^2}{2 N_0 B} = \gamma_{\rm OPC,UB}^{\rm double}(r). \tag{92}$$

REFERENCES

[1] Cisco Visual Networking Index, "Global mobile data traffic forecast update, 2014-2019," White Paper, Feb. 2015. [Online]. Available: http://www.cisco.com/c/en/us/solutions/collateral/service-provider/visual-networking-index-vni/white_paper_c11-520862.html

[2] N. Chi, H. Haas, M. Kavehrad, T. D. C. Little, and X. L. Huang, "Visible light communications: Demand factors, benefits and opportunities [Guest Editorial]," *IEEE Wireless Commun.*, vol. 22, no. 2, pp. 5–7, Apr. 2015.

[3] H. Chun *et al.*, "LED based wavelength division multiplexed 10 Gb/s visible light communications," *J. Lightw. Technol.*, vol. 34, no. 13, pp. 3047–3052, Jul. 2016.

[4] M. Islim *et al.*, "Towards 10 Gb/s orthogonal frequency division multiplexing-based visible light communication using a GaN violet microLED," *Photon. Res.*, vol. 5, no. 2, pp. A35–A43, Apr. 2017.

[5] S. Hussain, M. Abdallah, and K. Qaraqe, "Hybrid radio-visible light downlink performance in RF sensitive indoor environments," in *Proc. 6th Int. Symp. Commun., Control Signal Process.*, Athens, Greece, May 2014, pp. 81–84.

[6] V. Chandrasekhar, J. Andrews, and A. Gatherer, "Femtocell networks: A survey," *IEEE Commun. Mag.*, vol. 46, no. 9, pp. 59–67, Sep. 2008.

[7] J. T. J. Penttinen, *The Telecommunications Handbook: Engineering Guidelines for Fixed, Mobile and Satellite Systems*. New York, NY, USA: Wiley, 2015.

[8] T. Borogovac, M. Rahaim, and J. B. Carruthers, "Spotlighting for visible light communications and illumination," in *Proc. IEEE Globecom Workshops*, Miami, FL, USA, Dec. 2010, pp. 1077–1081.

[9] I. Stefan, H. Burchardt, and H. Haas, "Area spectral efficiency performance comparison between VLC and RF femtocell networks," in *Proc. IEEE Int. Conf. Commun.*, Budapest, Hungary, Jun. 2013, pp. 1–5.

[10] C. Chen, N. Serafimovski, and H. Haas, "Fractional frequency reuse in optical wireless cellular networks," in *Proc. IEEE 24th Int. Symp. Pers. Indoor Mobile Radio Commun.*, London, U.K., Sep. 2013, pp. 3594–3598.

[11] C. Chen, D. Tsonev, and H. Haas, "Joint transmission in indoor visible light communication downlink cellular networks," in *Proc. IEEE Globecom Workshops*, Atlanta, GA, USA, Dec. 2013, pp. 1127–1132.

[12] Z. Chen and H. Haas, "Space division multiple access in visible light communications," in *Proc. IEEE Int. Conf. Commun.*, London, U.K., Jun. 2015, pp. 5115–5119.

[13] J. Carruthers and J. Kahn, "Angle diversity for nondirected wireless infrared communication," *IEEE Trans. Commun.*, vol. 48, no. 6, pp. 960–969, Jun. 2000.

[14] Y. Alqudah and M. Kavehrad, "Optimum order of angle diversity with equal-gain combining receivers for broad-band indoor optical wireless communications," *IEEE Trans. Veh. Technol.*, vol. 53, no. 1, pp. 94–105, Jan. 2004.

[15] H. L. Minh *et al.*, "A 1.25-Gb/s indoor cellular optical wireless communications demonstrator," *IEEE Photon. Technol. Lett.*, vol. 22, no. 21, pp. 1598–1600, Nov. 2010.

[16] M. Alresheedi and J. Elmirghani, "Performance evaluation of 5 Gbit/s and 10 Gbit/s mobile optical wireless systems employing beam angle and power adaptation with diversity receivers," *IEEE J. Sel. Areas Commun.*, vol. 29, no. 6, pp. 1328–1340, Jun. 2011.

[17] A. Nuwanpriya, S. W. Ho, and C. S. Chen, "Indoor MIMO visible light communications: Novel angle diversity receivers for mobile users," *IEEE J. Sel. Areas Commun.*, vol. 33, no. 9, pp. 1780–1792, Sep. 2015.

[18] Z. Chen, D. Tsonev, and H. Haas, "Improving SINR in indoor cellular visible light communication networks," in *Proc. IEEE Int. Conf. Commun.*, Sydney, NSW, Australia, Jun. 2014, pp. 3383–3388.

[19] Z. Chen, D. Tsonev, and H. Haas, "A novel double-source cell configuration for indoor optical attocell networks," in *Proc. IEEE Global Commun. Conf.*, Austin, TX, USA, Dec. 2014, pp. 2125–2130.

[20] J. M. Kahn and J. R. Barry, "Wireless infrared communications," *Proc. IEEE*, vol. 85, no. 2, pp. 265–298, Feb. 1997.

[21] J. Barry, J. Kahn, W. Krause, E. Lee, and D. Messerschmitt, "Simulation of multipath impulse response for indoor wireless optical channels," *IEEE J. Sel. Areas Commun.*, vol. 11, no. 3, pp. 367–379, Apr. 1993.

[22] S. Vasudevan, K. Papagiannaki, C. Diot, J. Kurose, and D. Towsley, "Facilitating access point selection in IEEE 802.11 wireless networks," in *Proc. ACM 5th SIGCOMM Conf. Internet Meas.*, Berkeley, CA, USA, Oct. 2005, pp. 293–298.

[23] J. Winters, "Optimum combining in digital mobile radio with cochannel interference," *IEEE J. Sel. Areas Commun.*, vol. SAC-2, no. 4, pp. 528–539, Jul. 1984.

[24] A. Jalajakumari, K. Cameron, D. Tsonev, H. Haas, and R. Henderson, "An energy efficient high-speed digital LED driver for visible light communications," in *Proc. IEEE Int. Conf. Commun.*, London, U.K., Jun. 2015, pp. 5054–5059.

[25] Z. Chen and H. Haas, "A simplified model for indoor optical attocell networks," in *Proc. IEEE Summer Topicals Meeting Ser.*, Nassau, Bahamas, Jul. 2015, pp. 167–168.

[26] C. Chen, D. Basnayaka, and H. Haas, "Downlink performance of optical attocell networks," *J. Lightw. Technol.*, vol. 34, no. 1, pp. 137–156, Jan. 2016.

[27] R. H. Simons and A. Bean, *Lighting Engineering: Applied Calculations.* New York, NY, USA: Architectural Press, 2008.

[28] F. E. Alsaadi and J. M. H. Elmirghani, "Mobile MC-CDMA optical wireless system employing an adaptive multibeam transmitter and diversity receivers in a real indoor environment," in *Proc. IEEE Int. Conf. Commun.*, Beijing, China, May 2008, pp. 5196–5203.

[29] Z. Cao, L. Shen, Y. Jiao, X. Zhao, and T. Koonen, "200 Gbps OOK transmission over an indoor optical wireless link enabled by an integrated cascaded aperture optical receiver," in *Proc. Opt. Fiber Commun. Conf. Exhib.*, Los Angeles, CA, USA, Mar. 2017, pp. 1–3.

[30] C. Chen, S. Videv, D. Tsonev, and H. Haas, "Fractional frequency reuse in DCO-OFDM-based optical attocell networks," *J. Lightw. Technol.*, vol. 33, no. 19, pp. 3986–4000, Oct. 2015.

Zhe Chen (S'14–M'17) received the B.Eng. degree in communication system engineering (first class hons.) from the University of Birmingham, Birmingham, U.K., in 2011, the M.Sc. degree in signal processing and communications from the University of Edinburgh, Edinburgh, U.K., in 2012, and the Ph.D. degree in digital communications from the University of Edinburgh, Edinburgh, U.K., in 2016. He is currently with Fujitsu Research & Development Centre, Beijing, China. His current research interests include interference mitigation, angle diversity, and multiple-input multiple-output techniques in 5G-NR systems. He was a recipient of the scholarship from EPSRC-funded ultraparallel visible light communications project for his doctoral studies.

Dushyantha A. Basnayaka (S'11–M'12–SM'18) received the B.Sc. Eng. degree (first hons.) and the Ph.D. degree in electrical and electronics engineering in 2006 and 2012, respectively. He is currently with the Institute for Digital Communications, The University of Edinburgh, Edinburgh, U.K. His research interests include multiple-input multiple-output, physical layer aspects of Internet of Things (IoT) and 5G, and visible light communication systems. He holds three patents (one granted and two pending) in CoMP and IoT. He was a recipient of the University of Canterbury International Doctoral Scholarship from 2009 to 2012 and the Best Paper Award at the IEEE Vehicular Technology Conference (Spring) in 2015.

Xiping Wu (S'11–M'14) received the B.Sc. degree from Southeast University, Nanjing, China, in 2008, and the M.Sc. (with distinction) and Ph.D. degrees from the University of Edinburgh, Edinburgh, U.K., in 2011 and 2015, respectively. From September 2011 to August 2014, he was a Marie-Curie Early-Stage Researcher, funded by the European Union's Seventh Framework Programme project GREENET. From December 2013 to April 2014, he was on secondment to the Department of Electrical and Information Engineering, University of LAquila, LAquila, Italy. He is currently a Research Associate with the Institute for Digital Communications, The University of Edinburgh, funded by the British Engineering and Physical Sciences Research Council project TOUCAN. His main research interests include wireless communication theory, visible light communications, and wireless network management. He was the recipient of the Scotland Saltire Scholarship by the Scottish Government in 2010.

Harald Haas (S'98–A'00–M'03–SM'17–F'18) received the Ph.D. degree from the University of Edinburgh, Edinburgh, U.K., in 2001. He currently holds the Chair of Mobile Communications, The University of Edinburgh, and is the initiator, cofounder, and Chief Scientific Officer with pureLiFi Ltd., as well as the Director of the LiFi Research and Development Center, The University of Edinburgh. His main research interests include optical wireless communications, hybrid optical wireless and radio frequency communications, spatial modulation, and interference coordination in wireless networks. He first introduced and coined spatial modulation and LiFi. LiFi was listed among the 50 best inventions in TIME Magazine 2011. He was an invited speaker at TED Global 2011, and his talk, Wireless Data from Every Light Bulb, has been watched online more than 2.5 million times. He gave a second TED Global lecture in 2015 on the use of solar cells as LiFi data detectors and energy harvesters. This has been viewed online more than 2.1 million times. He authored or coauthored more than 430 conference and journal papers including a paper in *Science*. In 2012 and 2017, he was the recipient of the prestigious Established Career Fellowship from the Engineering and Physical Sciences Research Council (EPSRC) within Information and Communications Technology in the U.K. In 2014, he was selected by the EPSRC as one of ten Recognising Inspirational Scientists and Engineers Leaders in the U.K. In 2016, he was a recipient of the Outstanding Achievement Award from the International Solid State Lighting Alliance. He became a Fellow of the Royal Society of Edinburgh in 2017. In the same year, he was a recipient of the Wolfson Research Merit Award from the Royal Society.